RSC Advances

ROYAL SOCIETY OF CHEMISTRY

www.rsc.org/advances

Journal Name

COMMUNICATION

Direct synthesis of Co@Al-MCM-41 catalyst from conventional Co/SiO_2 catalyst†

Received 00th January 20xx,
Accepted 00th January 20xx

DOI: 10.1039/x0xx00000x

www.rsc.org/

Jiang-Yong Liu, [a] Jian-Feng Chen *[a] and Yi Zhang *[a]

A Co@Al-MCM-41 catalyst was directly synthesized from Co/SiO_2 catalyst. Various characterization results demonstrate that Co_3O_4 particles, from the Co/SiO_2 catalyst, were compatibly imbedded and firmly confined into the crystal of Al-MCM-41. The suitable cobalt particle size and acidity of zeolite realized as high as 64.5% selectivity of gasoline in Fischer-Tropsch synthesis. Meanwhile, the excellent stability was confirmed.

The M41S family of mesoporous molecular sieves, with well-defined pore structure and large surface area, has aroused great attention since the first discovery by the Mobil researchers.[1–2] The most extensively studied member is MCM-41, which consists of a unidimensional and hexagonal array of mesopores.[3] However, the neutral character of the purely siliceous MCM-41 limits its application in the catalytic processes such as hydrocracking and isomerization. For the generation of acidic sites, tremendous efforts have been devoted to the incorporation of aluminum into the MCM-41 framework.[4] In addition, the substitution of aluminum for silicon in the mesopore wall can effectively promote the hydrothermal stability of the pure MCM-41 material.[5]

The Fischer-Tropsch synthesis (FTS) is a heterogeneous catalytic process for the production of clean fuel via the transformation of syngas (mixture of CO and H_2).[6–7] The FTS hydrocarbon products obey the Anderson-Schulz-Flory (ASF) distribution, and therefore a maximum selectivity for the desired range of hydrocarbons is theoretically limited.[8] The development of novel catalysts with high activity and good selectivity remains the key to improving the FT technologies. Owing to its excellent physical properties derived from the unique periodic mesoporous silicas, MCM-41 has been generally employed as the support for the preparation of Co-based, Fe-based and Ru-based catalysts in the FTS reaction.[9–11] However, these research mainly focused on elaborating the influence of support porous structure (pore size, texture effect, etc.) and the active metal properties (metal size, metal dispersion, etc.) on the catalytic behavior. In addition, the FTS reaction performances of these MCM-41 supported catalysts were usually unsatisfactory, with high methane selectivity and unstable catalytic activity. Different from the conventional microporous zeolites,[12, 13] few studies have been reported regarding the detailed application of MCM-41-based catalysts in the FTS contributing to form a target product or a specific range of hydrocarbons. Herein, not limited to the microporous HZSM-5, we directly synthesized Co@Al-MCM-41 catalyst with imbedded structure from conventional Co/SiO_2 catalyst, in order to effectively adjust the product distribution of FTS and obtain gasoline range hydrocarbons.

For the preparation of Co@Al-MCM-41, cetyltrimethylammonium bromide (CTAB) was employed as a template surfactant. The dissolved silica from precursor Co/SiO_2 was the only Si source, and $Al(NO_3)_3{\cdot}9H_2O$ was selected as the Al source. The catalyst was synthesized with the following molar composition: 1.0 SiO_2 (Co/SiO_2): 0.125 CTAB: 0.02 Al: 0.30 TMAOH: 8.0 NH_3: 50.0 H_2O. In a typical procedure, CTAB was firstly dissolved in water, and then TMAOH, $Al(NO_3)_3{\cdot}9H_2O$, Co/SiO_2 and $NH_3{\cdot}H_2O$ were added successively. After hydrothermal crystallization, filtration, washing and calcination, the Co@Al-MCM-41 catalyst can be thus obtained (see the ESI†). During the hydrothermal process, the gradually dissolved silica from Co/SiO_2 and Al species crystallized to form the Al-MCM-41 framework while the remaining Co_3O_4 particles served as a substrate for the nucleation and growth of Al-MCM-41 crystals.

Fig. S1 (ESI†) presents the SA-XRD profiles of the pure Al-MCM-41, the precursor Co/SiO_2, the impregnated Co/Al-MCM-41 catalyst and the cobalt-imbedded Co@Al-MCM-41 catalyst. As can be seen, the pure Al-MCM-41 exhibits three distinct diffraction peaks indexed to the (100), (110), (200) planes, corresponding to a hexagonal structure with the *P6mm* space group,[14] and thus a highly ordered mesoporous structure was achieved. The *d* spacing values and the hexagonal unit cell parameter a_0 are given in Table S1 (ESI†). The TEM images in Fig. S2 (ESI†) also illustrate a highly ordered mesopore organization of the pure mesoporous Al-MCM-41. Additional information about the mesoporous properties can be obtained from the N_2 adsorption-desorption isotherms (Fig. S3a,

[a] State Key Laboratory of Organic-Inorganic Composites; Research Centre of the Ministry of Education for High Gravity Engineering and Technology; Beijing University of Chemical Technology, Beijing 100029, China
E-mail: chenjf@mail.buct.edu.cn, yizhang@mail.buct.edu.cn

† Electronic Supplementary Information (ESI) available: Experimental section, detailed discussion, supporting results and some characterization techniques such as SA-XRD, WA-XRD, TEM, N_2 adsorption–desorption, [27] Al MAS NMR, NH_3-TPD, H_2-TPR and XPS. See DOI: 10.1039/x0xx00000x

ESI†). It can be seen that the pure Al-MCM-41 support presents a type IV isotherm, characteristic of the uniform mesoporous material according to the IUPAC nomenclature, further demonstrating its excellent structure ordering.[15] Moreover, the corresponding pore size distribution calculated from the desorption branch by the BJH model displays one narrow distribution peak. For the supported Co/Al-MCM-41 catalyst, the decrease in the intensity of the (100) reflection and its broadening, together with the disappearance of the other small diffraction peaks indicate that a lowering in the structure regularity took place after the calcination process.[10,16] What's more, a significant decrease in the surface area and the pore volume is observed, which can be attributed to the pore blockage [17] by the cobalt oxide particles and the effect of silica "dilution" [18] due to the presence of cobalt species. The TEM and the STEM investigations provide the direct observation of the morphology and distribution of Co_3O_4 particles in the Co/Al-MCM-41 catalyst, as displayed in Fig. 1(a) and Fig. 2b, respectively. It can be observed that the small Co_3O_4 particles were highly dispersed along the mesoporous channels, where part of the pore openings were obstructed and thus demonstrated the presence of pore blocking. Therefore, it is supposed that the cobalt deposition and subsequent calcination resulted in a deterioration of the textural characteristics of the mesopores of Al-MCM-41. Meanwhile, highly dispersed cobalt, namely small cobalt particles, would contribute to forming light hydrocarbon products, especially methane.

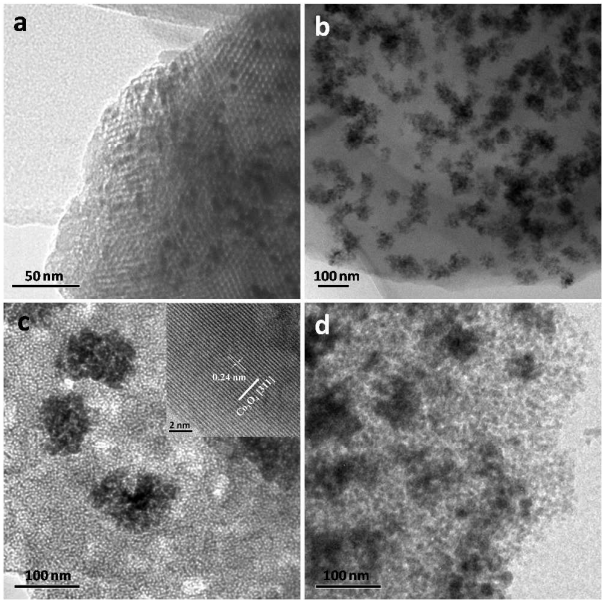

Fig. 1. TEM images of (a) the Co/Al-MCM-41 catalyst, (b, c) the Co@Al-MCM-41 catalyst and (d) the Co/SiO2 catalyst. The inset in (c) is the HRTEM image of the Co_3O_4 phase.

Different from those of the Co/Al-MCM-41 catalyst, the TEM images (Fig. 1b, c) and the STEM images (Fig. 2a, c) of the Co@Al-MCM-41 catalyst show that the cobalt oxide particles are present in clusters, which is same with that of the Co/SiO_2 catalyst. On the other hand, the cobalt clusters are compatibly imbedded or confined in the mesoporous silica framework. What's more, the STEM-EDS analysis and the elemental mapping (Fig. 2d-f) clearly provide a direct insight into this cobalt-imbedded structure. And the textural mesoporosity and the long-range ordering of the Co@Al-MCM-41 catal-yst was still retained to a large extent, confirmed by the well-defined (100) diffraction peak (Fig. S1d, ESI†). As shown in Fig. S3b (ESI†), the Co@Al-MCM-41 sample with cobalt-imbedded structure still exhibits a N_2 adsorption-desorption isotherm with satisfactory mesoporous character. It is worth noting that an additional step is observed in a relative pressure of 0.95-1.0 and can be ascribed to the existence of the void defects (Fig. 1c and Fig. 2c) in the framework of Al-MCM-41, which can make the nanochannels highly interconnected and therefore can improve the diffusion of the reactive molecules (See Fig. S3 and detailed discussion).[19]

Fig.S4 (ESI†) shows the WA-XRD profiles of the samples. The pure Al-MCM-41 exhibits only one broad band centered at about 20°caused by the amorphous silica walls, and no other diffraction peaks are present, similar with SiO_2. For all the cobalt-containing samples, well-resolved XRD diffractions were obtained, with only spinel Co_3O_4 phase detected.[20, 21] Compared with those of the Co@Al-MCM-41 catalyst, the diffraction peaks of the Co/Al-MCM-41 catalyst are obviously lower and broader, suggesting a significantly smaller Co_3O_4 particle size. The properties of the obtained catalysts were compared in Table S2 (ESI†). After the hydrothermal treatment, the average Co_3O_4 and cobalt metal particle size of the Co@Al-MCM-41 catalyst has almost no change with that of the Co/SiO_2 precursor, revealing that the Co particles were eventually imbedded or confined in the mesoporous silica, contributing to realizing excellent reaction performance of FTS.

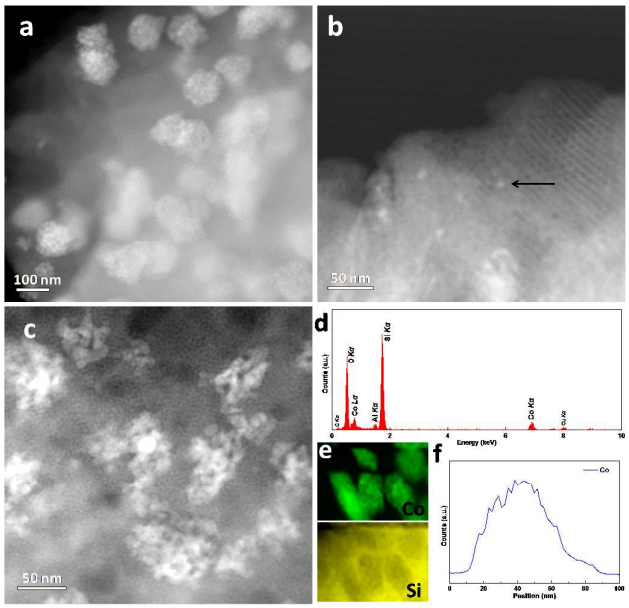

Fig. 2. STEM images of the samples: (a, c) Co@Al-MCM-41 (b) Co/Al-MCM-41. (d) The EDS spectrum of the Co@Al-MCM-41 catalyst. (e) and (f) are the EDS elemental mapping and the line-scan analysis of a single Co_3O_4 cluster of the Co@Al-MCM-41 catalyst, respectively.

The elemental composition of the samples was determined by the XRF analysis. As shown in Table S1 (ESI†), the cobalt content of all the catalysts resembles with that of the theoretical value, i.e. 20 wt%. The bulk molar ratios of Si/Al of all the samples are in the range of 45-47 and close to the nominal value (50) of the primary

synthetic solution. These observations imply the high utilization efficiency of silica and aluminum species in the reaction mixture. When a trivalent Al^{3+} substitutes for Si^{4+}, the framework possesses a negative charge that can be compensated by a proton to form a Brönsted acidic site, which is an essential precondition for a variety of acid-catalyzed reactions, like the cracking reaction of long-chain hydrocarbons.[22] The quality, location and coordination state of aluminum in the samples were also investigated by the ^{27}Al MAS NMR experiment (See Fig. S5 and detailed discussion, ESI†). And the acidic property was further investigated by the NH_3-TPD method (Fig. S6, ESI†). The NH_3-TPD profile of Co/SiO_2 shows only one peak, which is very weak and locates at low temperature, corresponding to the desorption of NH_3 from the weak acidic sites. For the other two catalysts, the high-temperature peak can be ascribed to the medium acidic sites. The higher intensity of this additional peak indicates that the Co/Al-MCM-41 catalyst possesses more acidic sites, while the higher desorption temperature demonstrates it has stronger surface acidity.[23-25]

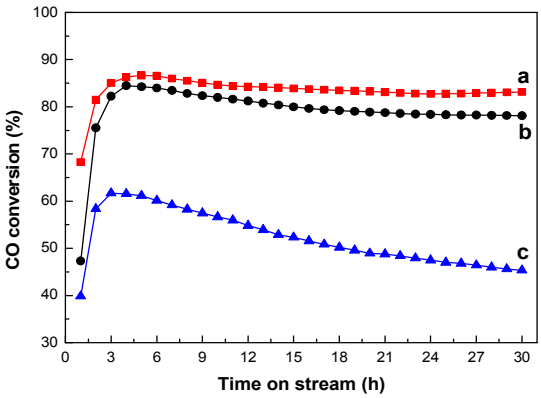

Fig. 3. CO conversion with time on stream over the catalysts: (a) Co/SiO_2; (b) Co@Al-MCM-41; (c) Co/Al-MCM-41. Reaction conditions: 1.0 MPa, 523 K, molar ratio of H_2/CO = 2.0, W/F=5.0 g-cat.h/mol

The H_2-TPR experiment was performed to investigate the reducibility of the cobalt-based catalysts (See Fig. S7 and detailed discussion, ESI†). The results indicate that the cobalt phase in the supported Co/Al-MCM-41 catalyst has a very intense mutual interaction with the Al-MCM-41 support, and thus a lot of inactive cobalt silicate and cobalt aluminate species can be generated, giving rise to the poor reducibility of this catalyst. This extremely strong interaction can also be evidenced by the XPS results (See Fig. S8 and detailed discussion, ESI†). Furthermore, compared with the Co/Al-MCM-41 catalyst, the Co@Al-MCM-41 catalyst presents a much lower intensity of the $Co2p_{3/2}$ and $Co2p_{1/2}$ peaks, indicating that cobalt oxides were almost all imbedded or confined into the Al-MCM-41 mesoporous silica since XPS is known as a surface-sensitive technique.[26]

The FTS reaction results of the different catalysts were compared in Table S3 (ESI†). As expected, the conventional Co/SiO_2 catalyst exhibited a high CO conversion of 83.1 %. The low catalytic activity of the supported Co/Al-MCM-41 catalyst can be reasonably attributed to its poor reducibility, which would form less cobalt metallic active sites. Furthermore, the diffusion barrier of the CO and H_2 molecules should be taken into consideration. In the case of the Co/Al-MCM-41 catalyst, the external syngas must pass through the unidimensional mesoporous channels to contact the highly dispersed Co^0 active sites. And the diffusion difficulty can be further aggravated since some pores were blocked by the tiny cobalt particles. Nevertheless, different from this structure feature, the diffusion restriction in the Co@Al-MCM-41 catalyst with cobalt-imbedded structure can be significantly alleviated since the reactive molecules can diffusion along all directions to react with the large metal clusters. Furthermore, the void defects in the Al-MCM-41 framework of the Co@Al-MCM-41 catalyst can enhance the diffusion rate of the syngas. In addition, the Co@Al-MCM-41 catalyst presents a much better reducibility than the Co/Al-MCM-41 catalyst. All these findings can be rationally applied to explain the high catalytic activity of the Co@Al-MCM-41 catalyst.

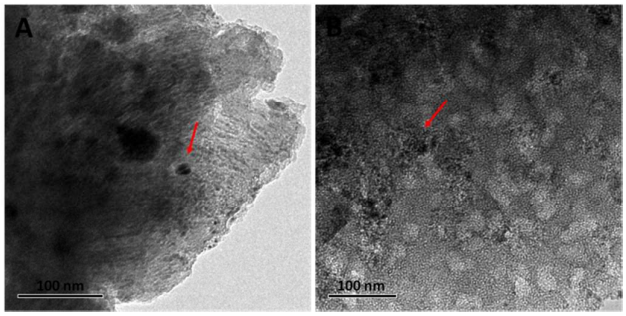

Fig. 4. TEM images of the spent catalysts: (a) Co/Al-MCM-41, (b) Co@Al-MCM-41

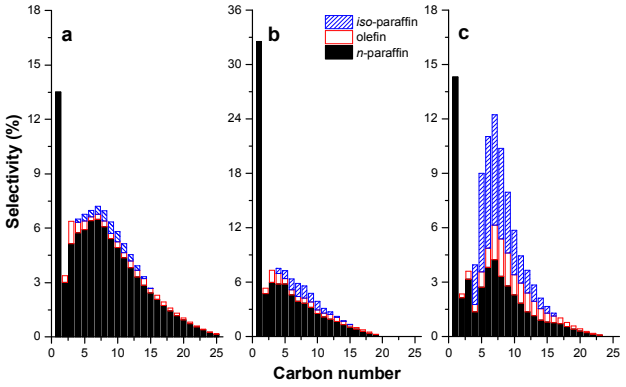

Fig. 5. FTS product distribution of various catalysts: (a) Co/SiO2, (b) Co/Al-MCM-41, (c) Co@Al-MCM-41.

Fig. 3 compares the catalytic activity of three different kinds of catalysts with time-on-stream (TOS). For the three reactions, the observed stability decreased in the order of Co/SiO_2 > Co@Al-MCM-41 > Co/Al-MCM-41. Specifically, the impregnated Co/Al-MCM-41 catalyst undergoes a fast deactivation during the reaction duration, which could be due to the easily re-oxidized and sintered small cobalt particles,[27,28] and thus a lot of Co^0 active sites were gradually lost as the reaction proceeded. Moreover, the low transportation efficiency of the produced water would aggravate this oxidization

process. In addition, the hydrolysis and deterioration of the pore structure occurred as supported by the SA-XRD profile (Fig. S9A, ESI†) and TEM image (Fig. 4a) of the spent Co/Al-MCM-41 catalyst. However, compared with the Co/Al-MCM-41 catalyst, the Co@Al-MCM-41 catalyst presents a much better stability. After reaction, the spent Co@Al-MCM-41 catalyst still displays a satisfactory textural mesoporosity, which can be reasonably attributed to the larger cobalt size, the better diffusion efficiency and the acid-catalyzed reactions (hydrocracking, isomerization, etc) of the waxy hydrocarbons that could form the coke accumulation. It should be noted that the reaction temperature of 523 K is appropriate for these acid-catalyzed reactions on the Co@Al-MCM-41 catalyst since the XRD peaks (Fig. S10B, ESI†) of residual long-chain paraffin wax [29,30] were not observed, but these peaks could be detected after the FTS reaction at 503 K.

As expected, the Co/SiO_2 catalyst shows a conventional wide product distribution (Table S3, ESI† and Fig. 5), with C_{20+} products. The Co/Al-MCM-41 catalyst exhibits a significantly higher selectivity of methane (32.6%). There are several factors that can contribute to the high CH_4 selectivity in the Co/Al-MCM-41 catalyst (ESI†, detailed discussion). It should be noted that the Co@Al-MCM-41 catalyst presented a highest selectivity of gasoline-range hydrocarbons, which should be ascribed to the promotional effect of the desired confined reaction environment derived from the cobalt-imbedded structure. In comparison with the Co/Al-MCM-41 catalyst, the relatively larger cobalt particles of the Co@Al-MCM-41 catalyst are prone to obtain the long-chain hydrocarbons. Afterwards, in a typical process, the primary long-chain hydrocarbons can be effectively transformed and controllably converted into the light isoparaffins by the secondary hydrocracking and isomerization reactions due to the acidic properties of the aluminum-containing mesoporous silica, which contributes to suppressing the selectivity of waxy paraffins and facilitate the selectivity of gasoline-range hydrocarbons.

Conclusions

In conclusion, the cobalt-imbedded Al-MCM-41 catalyst was developed in this study and presented excellent multiple functionalities. The application of this imbedment-structured catalyst to the Fischer-Tropsch synthesis gave a satisfactory selectivity of gasoline-range hydrocarbons, which reached up to 64.5 % at CO conversion of 78.1 %. In addition, this tailor-made Co@Al-MCM-41 catalyst exhibited a high catalytic activity and a good stability during the reaction duration. Characterization results suggested that the remarkable catalytic performance of the Co@Al-MCM-41 catalyst can be rationally ascribed to the desired confined reaction environment, which provides us a new approach to tune the product distribution of the Fischer-Tropsch synthesis.

Acknowledgements

We gratefully acknowledge the financial support from the National Natural Science Foundation of China (91334206, 51174259), Ministry of Education (NCET-13-0653), National “863” program of China (2013AA031702) and Innovation and Promotion Project of Beijing University of Chemical Technology.

Notes and references

1. C. T. Kresge, M. E. Leonowicz, W. J. Roth, J. C. Vartuli and J. S. Beck, *Nature*, 1992, **359**, 710–712.
2. J. S. Beck, J. C. Vartuli, W. J. Roth, M. E. Leonowicz, C. T. Kresge, K. D. Schmitt, T. W. Chu, D. H. Olson and E. W. Sheppard, *J. Am. Chem. Soc.*, 1992, **114**, 10834–10843.
3. R. Nejat, A. R. Mahjoub, Z. Hekmatian and T. Azadbakht, *RSC Adv.*, 2015, **5**, 16029–16035.
4. J. Dědeček, N. Žilková and J. Čejka, *Microporous Mesoporous Mater.*, 2001, **44**, 259–266.
5. R. Mokaya, *J. Phys. Chem. B*, 2000, **104**, 8279–8286.
6. X. Chen, D. Deng, X. Pan, Y. Hu and X. Bao, *Chem. Commun.*, 2015, **51**, 217–220.
7. O. O. James, B. Chowdhury, M. A. Mesubi and S. Maity, *RSC Adv.*, 2012, **2**, 7347–7366.
8. H. M. Torres Galvis, J. H. Bitter, C. B. Khare, M. Ruitenbeek, A. I. Dugulan and K. P. de Jong, *Science*, 2012, **335** , 835–838.
9. A. Y. Khodakov, A. Griboval-Constant, R. Bechara and V. L. Zholobenko, *J. Catal.*, 2002, **206**, 230–241.
10. A. Y. Khodakov; V. L. Zholobenko, R. Bechara and D. Durand, *Microporous Mesoporous Mater.*, 2005, **79**, 29–39.
11. A. Y. Khodakov, A. Griboval-Constant, R. Bechara and F. Villain, *J. Phys. Chem. B*, 2001, **105**, 9805–9811.
12. J. Bao, J. He, Y. Zhang, Y. Yoneyama and N. Tsubaki, *Angew. Chem., Int. Ed.*, 2008, **47**, 353–356.
13. J. Y. Liu, J. F., Chen and Y. Zhang, *Catal. Sci. Technol.*, 2013**, 3,** 2559–2564.
14. W. H. Zhang, X. B. Lu; J. H. Xiu, Z. L. Hua, L. X. Zhang, M. Robertson, J. L. Shi, D. S. Yan and J. D. Holmes, *Adv. Funct. Mater.*, 2004, **14**, 544–552.
15. M. R. Mello, D. Phanon, G. Q. Silveira, P. L. Llewellyn and C. M. Ronconi, *Microporous Mesoporous Mater.*, 2011**, 143**, 174–179.
16. Z. Gholami, A. Z. Abdullah and K. T. Lee, *Appl. Catal., A*, 2014, **479**, 76–86.
17. B. Li, W. Ma, C. Han, J. Liu, X. Pang and X. Gao, *Microporous Mesoporous Mater.*, 2012, **156**, 73–79.
18. J. Hong, P. A. Chernavskii, A. Y. Khodakov and W. Chu, *Catal. Today*, 2009, **140**, 135–141.
19. H. P. Lin, S. T. Wong, C. Y. Mou and C. Y. Tang, *J. Phys. Chem. B*, 2000, **104**, 8967–8975.
20. H. P. Cong and S. H. Yu, *Cryst. Growth Des.*, 2009, **9**, 210–217.
21. L. Zhang, W. He, X. Xiang, Y. Li and F. Li, *RSC Adv.*, 2014, **4**, 43357–43365.
22. S. P. Naik, V. Bui, T. Ryu, J. D. Miller and W. Zmierczak, *Appl. Catal., A*, 2010, **381**, 183–190.
23. T. Klimova, M. Calderón and J. Ramírez, *Appl. Catal., A*, 2003, **240**, 29–40.
24. H. Kosslick, G. Lischke, B. Parlitz, W. Storek and R. Fricke, *Appl. Catal., A*, 1999, **184**, 49–60.
25. Z. Zhang, Y. Han, L. Zhu, R. Wang, Y. Yu, S. Qiu, D. Zhao and F. S. Xiao, *Angew. Chem., Int. Ed.*, 2001, **40**, 1258–1262.
26. A. Dangwal Pandey, C. Jia, W. Schmidt, M. Leoni, M. Schwickardi, F. Schüth and C. Weidenthaler, *J. Phys. Chem. C*, 2012, **116**, 19405–19412.
27. E. Iglesia, *Appl. Catal., A*, 1997, **161**, 59–78.
28. J. Scalbert , C. Legens, I. Clémençon, A. L.Taleb, L.Sorbier and F. Diehl, *Chem. Commun.*, 2014, **50**, 7866–7869.
29. L. Chen and J. Shen, *J. Catal.*, 2011, **279**, 246–256.
30. Y. Ohtsuka, Y. Takahashi, M. Noguchi, T. Arai, S. Takasaki, N. Tsubouchi and Y. Wang, *Catal. Today*, 2004, **89**, 419–429.

Direct synthesis of Co@Al-MCM-41 catalyst from conventional Co/SiO_2 catalyst†

Jiang-Yong Liu, [a] Jian-Feng Chen *[a] and Yi Zhang *[a]

A Co@Al-MCM-41 catalyst directly synthesized from Co/SiO_2 realized high selectivity of gasoline in Fischer-Tropsch synthesis with excellent stability due to suitable cobalt particle size and acidity of zeolite